© 2022. Published by The Company of Biologists Ltd | Development (2022) 149, dev200953. doi:10.1242/dev.200953

RESEARCH REPORT

Dentate gyrus morphogenesis is regulated by β-catenin function in hem-derived fimbrial glia

Arpan Parichha[1], Debarpita Datta[1], Varun Suresh[1], Mallika Chatterjee[2], Michael J. Holtzman[3] and Shubha Tole[1,*]

ABSTRACT

The dentate gyrus, a gateway for input to the hippocampal formation, arises from progenitors in the medial telencephalic neuroepithelium adjacent to the cortical hem. Dentate progenitors navigate a complex migratory path guided by two cell populations that arise from the hem, the fimbrial glia and Cajal-Retzius (CR) cells. As the hem expresses multiple Wnt genes, we examined whether β-catenin, which mediates canonical Wnt signaling and also participates in cell adhesion, is necessary for the development of hem-derived lineages. We report that, in mice, the fimbrial glial scaffold is disorganized and CR cells are mispositioned upon hem-specific disruption of β-catenin. Consequently, the dentate migratory stream is severely affected, and the dentate gyrus fails to form. Using selective Cre drivers, we further determined that β-catenin function is required in the fimbrial glial scaffold, but not in the CR cells, for guiding the dentate migration. Our findings highlight a primary requirement for β-catenin for the organization of the fimbrial scaffold and a secondary role for this factor in dentate gyrus morphogenesis.

KEY WORDS: β-Catenin, Cajal-Retzius cells, Dentate gyrus, Dentate gyrus morphogenesis, Fimbrial scaffold, Hem-derived fimbrial glia, Mouse

INTRODUCTION

In the developing central nervous system, specialized cell types arising from discrete neuroepithelial domains perform important roles in guiding the assembly of particular brain structures. The cortical hem, a Wnt-rich structure in the embryonic medial telencephalon, produces several distinct lineages, including the telencephalic choroid plexus epithelium, Cajal-Retzius (CR) cells and glia that comprise the fimbrial scaffold (Louvi et al., 2007; Gu et al., 2011). Each of these lineages contributes either secreted factors or cellular substrates that perform important functions in neocortical and hippocampal development (Caramello et al., 2021; Bagri et al., 2002; Lehtinen et al., 2011). The molecular processes that operate within hem progenitors to modulate the development of these lineages are not well understood. We focused on β-catenin because it performs two distinct functions, as a transcription factor in the canonical Wnt pathway and also as part of the adherens complex at the cell membrane. Here, we examine the effect of loss of β-catenin on the development of the CR cells and the fimbrial glial scaffold.

Both, the CR cells and the fimbrial glial scaffold are essential in the regulation of dentate gyrus morphogenesis, a process that has been well characterized in rodents. Dentate gyrus granule neurons are produced in the dentate neuroepithelium (DNE), a region of the ventricular zone adjacent to the hem (Altman and Bayer, 1990a). Proliferating progenitors from the DNE as well as specified dentate granule cells migrate along a curved path called the dentate migratory stream (DMS; Altman and Bayer, 1990b), and eventually form the characteristic 'V' shaped gyrus at the hippocampal fissure. CR cells secrete chemokines that are crucial for the guidance of the DMS (Nakajima et al., 1997; Bagri et al., 2002; Lu et al., 2002). The migration of the CR cells is itself dependent on the fimbrial glial scaffold (Gu et al., 2011). This scaffold is crucial in guiding both the CR cells and the DMS, it is therefore important to understand how its organization and orientation are regulated. Factors that regulate the timing of formation (Caramello et al., 2021) or the extent of this scaffold (Barry et al., 2008) have been reported; however, mechanisms that control its organization have not yet been identified.

Here, we report that when β-catenin is lost in embryonic mouse hem, the resulting fimbrial glial scaffold is specified but is highly disorganized and protrudes ectopically into the ventricle. CR cells are specified, but mispositioned in the ectopic protrusion formed by the fimbrial glia. Dentate granule cells are also specified but their migration is profoundly disrupted, resulting in the absence of a morphologically distinct dentate gyrus. These deficits do not appear if β-catenin is disrupted in the CR cells alone. Therefore, β-catenin function in the hem-derived fimbrial glial scaffold is necessary for its organization and, consequently, for the morphogenesis of the dentate gyrus.

RESULTS AND DISCUSSION

Lmx1aCre identifies hem-derived cell types

Lmx1a expression was seen in the embryonic day (E)12.5 cortical hem and the choroid plexus (Fig. 1A). An Ai9 reporter (a line carrying a stop-floxed tdTomato cassette) driven by Lmx1aCre (Chizhikov et al., 2010) labeled the hem and its derivatives including BLBP+ (Fabp7+) fimbrial glia and reelin+ CR cells at E12.5 and E18.5 (Fig. 1B-D). Dentate granule cells, identified by PROX1 labeling, do not display Ai9 fluorescence as they are not derived from the hem (Fig. 1C,D; Caramello et al., 2021).

β-Catenin loss of function in the hem disrupts the fimbrial glial scaffold and perturbs CR cell migration

The gene encoding β-catenin *(Ctnnb1)* is expressed throughout the telencephalic midline neuroepithelium at E12.5 (Fig. 1E,F) (Parichha et al., 2022; Kadowaki et al., 2007). A single cell RNA-sequencing

[1]Department of Biological Sciences, Tata Institute of Fundamental Research, Mumbai 400005, India. [2]Amity Institute of Neuropsychology and Neurosciences, Amity University, Noida, 201303, India. [3]Pulmonary and Critical Care Medicine, Washington University, St. Louis, MO 63110, USA.

*Author for correspondence (stole@tifr.res.in)

A.P., 0000-0002-5507-5742; D.D., 0000-0002-6643-769X; V.S., 0000-0002-9177-9843; M.C., 0000-0002-3656-5308; M.J.H., 0000-0001-8750-3716; S.T., 0000-0001-6584-443X

Handling Editor: François Guillemot
Received 24 May 2022; Accepted 22 September 2022

Development (2022) 149, dev200953. doi:10.1242/dev.200953

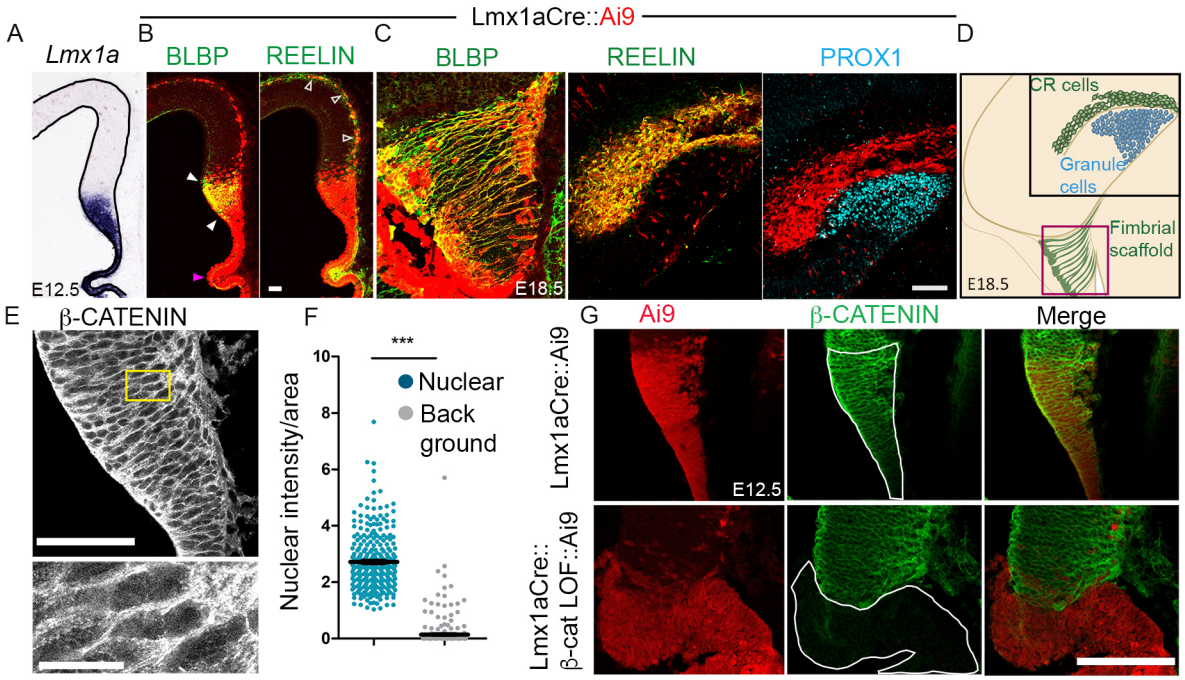

Fig. 1. Lmx1aCre identifies hem-derived lineages. (A) At E12.5 *Lmx1a* expression is seen in the hem and the choroid plexus. (B) Lmx1aCre drives Ai9 expression in the BLBP+ fimbrial glia (white arrowheads), the reelin+ CR cells (open arrowheads) and the choroid plexus epithelium (magenta arrowhead). (C) At E18.5 Ai9 fluorescence co-localizes with BLBP and reelin but not with dentate granule cell marker PROX1. (D) Cartoon illustrating the hem-derived lineages and dentate granule cells at E18.5. The black box indicates the region displayed in the reelin and PROX1 images and the magenta box represents the region displayed in the BLBP image in C. Representative images are shown of sections taken from *n*=5 brains (biologically independent replicates) examined over five independent experiments. (E,F) Immunostaining and quantification of nuclear β-catenin. Bottom panel in E shows magnification of yellow boxed area in top panel. ****P*<0.0001 (unpaired two-tailed *t*-test with Welch's correction). (G) β-Catenin is lost in Ai9-expressing cells in the Lmx1aCre::β-catenin LOF brain (white outline). Scale bars: 10 µm (E, magnification); 50 µm (B,C,E,G).

(scRNA-seq) study of E14.5 mouse cortex also identified *Ctnnb1* to be expressed in hem progenitors, CR cells and choroid plexus epithelium (Loo et al., 2019, GSE123335). We disrupted *Ctnnb1* in the developing hem using the Lmx1aCre driver together with a well-described mouse line in which exons 2-6 of the *Ctnnb1* gene are flanked by loxP sites and Cre-mediated recombination resulted in a non-functional transcriptionally inactive protein (Brault et al., 2001). In E12.5 Lmx1aCre::β-catenin loss-of-function (LOF) brains, the BLBP+ fimbrial glial scaffold was no longer confined to the region of the hem as it was in the controls (Fig. 2A-C; Fig. S1A). Instead, BLBP+ cells formed an ectopic protrusion into the ventricle just above the choroid plexus (Fig. 2B,C,E). We examined whether this protrusion arose as a result of excessive proliferation of the β-catenin LOF hem progenitors. However, both PHH3 and Ki67 immunostaining revealed no apparent change in proliferation (Fig. S1F-I).

One established function of the glial scaffold is to provide crucial cellular guidance to hem-derived CR cells in their migration to the marginal zone (MZ) of the hippocampus (Gu et al., 2011). Reelin immunostaining revealed many of these cells to be accumulated in the ectopically protruding fimbrial mass in Lmx1aCre::β-catenin LOF brains (Fig. 2C). We used a specific hem-derived CR cell marker, TRP73 to quantify the mislocalization of the CR cells (Fig. 2D; Fig. S1C). In E13.5 control brains, 95% of the CR cells occupied the MZ region and 5% were found outside this region, presumably en route to their final destination. Upon loss of β-catenin however, 56% were found in the MZ region and 43% were found outside the MZ (Fig. 2D,F; Fig. S1C-E).

The fimbrial glial scaffold dysmorphia seen in E12.5 β-catenin LOF brains did not improve with time but persisted at later stages in development (Fig. S1B, Fig. S2A). A comprehensive time-course panel from E11.5 to postnatal day (P)2 reveals misoriented fibers revealed by glial fibrillary acidic protein (GFAP) or BLBP labeling, in contrast to the well-organized alignment of these fibers in control brains (Fig. 2H; Fig. S2A,B). Reelin+ cells were mislocalized within the protruded glial mass at all stages examined (Fig. 2G; Fig. S2B).

In summary, loss of β-catenin in the hem resulted in striking defects in the organization of the fimbrial glial scaffold and in the migration of the CR cells, although both cell types appeared to be specified and displayed appropriate markers.

Transcriptional and adhesion-related roles of β-catenin in the hem

It is well established that β-catenin has two roles: it mediates transcriptional regulation in the canonical Wnt signaling pathway (Valenta et al., 2012) and also participates in adherens junctions, where it bridges the cadherins with the actin network (Gumbiner, 2005). Deletion of exon 2-6 of the *Ctnnb1* gene disrupts both functions (Valenta et al., 2011). No detectable β-catenin is seen in the Ai9-expressing cells in Lmx1aCre::β-catenin LOF brains (Fig. 1G). We performed RNA-seq analysis of the E12.5 control and β-catenin LOF hem (Fig. S3A-D). Gene ontology (GO) analysis shows GO:BP terms that include both 'Canonical Wnt signaling pathway' and 'Positive regulation of cell junction assembly' to be significantly downregulated upon loss of β-catenin, indicating that both functions of β-catenin may be relevant for fimbrial scaffold morphogenesis (Fig. S3C).

Several members of the canonical Wnt signaling pathway including *Fzd1*, *Tcf7l1*, *Tcf7l2*, *Axin2* and nuclear LEF1 were present in the E12.5 hem (Fig. S3E-G). Canonical Wnt targets

Development (2022) 149, dev200953. doi:10.1242/dev.200953

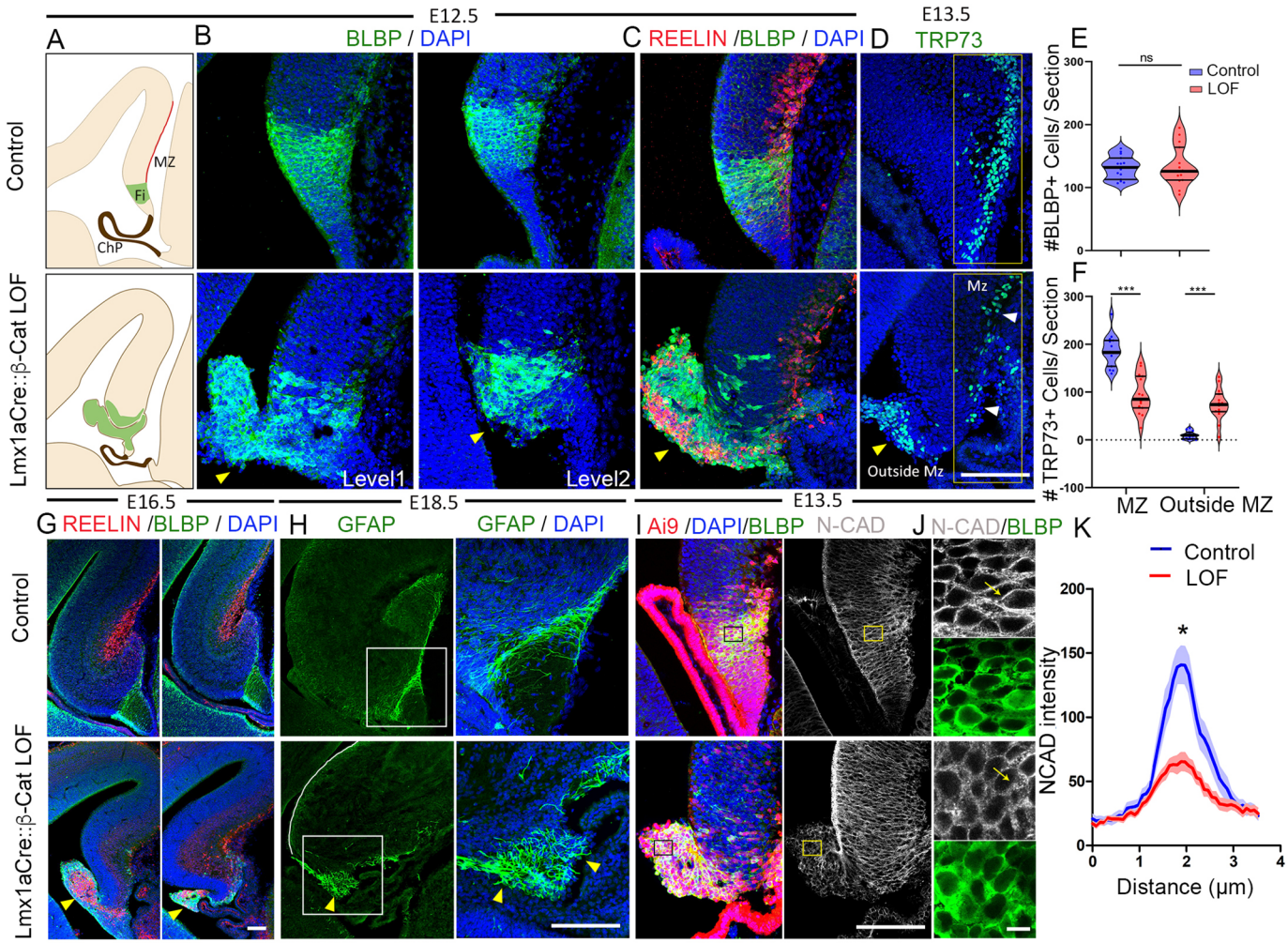

Fig. 2. Loss of β-catenin in the cortical hem causes disrupted assembly of the fimbrial scaffold and mispositioning of the CR cells. (A) Cartoons of E12.5 sections indicating the marginal zone (red line; MZ) and the fimbrial progenitors residing in the hem (green; Fi). ChP, choroid plexus. (B) BLBP immunostaining at two levels of sectioning reveals the disorganization of fimbrial scaffold and an ectopic glial protrusion (yellow arrowhead) in Lmx1aCre::β-catenin LOF brains in comparison with controls. Representative images are shown of sections taken from *n*=5 brains (biologically independent replicates) examined over five independent experiments. (C) Co-immunolabeling for reelin and BLBP reveals the mispositioning of CR cells in the ectopic glial protrusion (yellow arrowhead); representative images are shown of sections taken from *N*=3 brains (biologically independent replicates) examined over two independent experiments. (D) At E13.5, hem-derived TRP73+ CR cells are normally localized to the MZ (white arrowheads), but this population is significantly decreased in Lmx1aCre::β-catenin LOF brains and, instead, the cells are mislocalized in the ectopic glial protrusion (yellow arrowhead). (E) Quantification of BLBP+ cells shown in B reveals no significant difference in total BLBP+ cell number. (F) Quantification of TRP73+ cells shown in D indicates that 95% of the CR cells are localized in the MZ region in control brains, whereas only 56% are localized in the MZ in Lmx1aCre::β-catenin LOF brains and 44% are found outside the MZ region. *N*=5 brains (biologically independent replicates) examined over four independent experiments. (G) Co-immunolabeling with BLBP and reelin reveals the defective fimbrial scaffold in Lmx1aCre::β-catenin LOF brains at E16.5. (H) GFAP labeling at E18.5 reveals a well-ordered fimbrial scaffold in controls, but a disorganized scaffold in the Lmx1aCre::β-catenin LOF brains. Yellow arrowheads show the disorganized fimbrial scaffold. (I) Fimbrial scaffold cells identified by BLBP immunolabeling also display N-cadherin. (J) Magnification of the boxed region in I. (K) Quantification of N-cadherin across cell junctions along the yellow arrow in J. *n*=30 cells from *N*=3 brains (biologically independent replicates) examined over three independent experiments. Two-tailed unpaired Mann–Whitney *U*-test; **P*<0.05, ****P*<0.001; ns, *P*>0.05 (E: *P*=0.9268; F: *P*=0.007937; K: *P*=0.0150). Scale bars: 10 µm (J); 100 µm (B-D,G-I).

Pcsk6, *Fzd10*, *Runx2*, *Sost*, *Axin2* and *Wnt3* are significantly downregulated in the transcriptome of the β-catenin LOF hem (Fig. S3H; Table S1). We further validated that canonical Wnt targets *Axin2* and LEF1 are down regulated in β-catenin LOF hem by using *in situ* hybridization and immunohistochemistry, respectively (Fig. S3I,J). Finally, canonical Wnt signaling was implicated in the development of a different glial scaffold located at the dentate gyrus, which displayed defects upon loss of Wnt co-receptor LRP6 and transcriptional mediator LEF1 (Zhou et al., 2004). Together, these findings suggested that the fimbrial glial scaffold may require canonical Wnt signaling for normal development.

In contrast to the dysregulation of canonical Wnt targets, the mRNA and protein levels for fimbrial markers like GFAP, FABP7, ALDH1L1 and AQP4 did not differ significantly (Fig. S4A and B). Transcription factors SOX9, NFIA, and NFIB required for normal development of the fimbrial glial scaffold (Caramello et al., 2021; Bunt et al., 2017) are apparently unaltered in expression levels in upon loss of β-catenin (Fig. S4C and D).

To investigate the role of β-catenin in adhesion, we examined the distribution of N-cadherin (cadherin 2), a key member of cell-cell adherens junctions in neuroepithelium (Hirano and Takeichi, 2012) and enriched at the embryonic telencephalic midline (Kadowaki et al., 2007). We focused on the cell boundaries to assess the

Development (2022) 149, dev200953. doi:10.1242/dev.200953

junctional integrity of the control and mutant hem (E13.5; Fig. 2I-K) and fimbrial glial cells (E16.5; Fig. S5). Hem and fimbrial glial cells were identified by co-immunolabeling for BLBP. In the control, N-cadherin distribution measured along a linear path traversing two neighboring cells revealed a sharp peak in intensity at the boundary between the cells. In β-catenin LOF brains, there was a marked flattening of the peak intensity at cell boundaries, indicating a diffused distribution of N-cadherin and suggesting altered cell-cell adhesion, although the mRNA levels of *Cdh2*, which encodes N-cadherin, appeared to be unaltered (Fig. 2K; Fig. S5F,G).

These results suggested that the transcriptional dysregulation of factors that control fimbrial scaffold morphogenesis and/or perturbed cell adhesion as a result of altered N-cadherin distribution may underlie the disruption of the fimbrial glial scaffold resulting in the ectopic protrusion seen in β-catenin LOF brains. A comparison with β-catenin LOF selective to its transcriptional role, leaving its cell adhesion intact (Valenta et al., 2011), would be a useful additional study in this context and may help to identify novel β-catenin targets responsible for proper orientation and positioning of the fimbrial scaffold.

The dentate gyrus migratory stream is misdirected upon loss of β-catenin in the cortical hem, which leads to malformation of the dentate gyrus

That the fimbrial glial scaffold is specified but disorganized in Lmx1aCre::β-catenin LOF brains offered an opportunity to examine the effects of this perturbation on dentate morphogenesis. Dentate gyrus granule neurons are produced in the DNE and express PROX1, a factor necessary for their maturation (Lavado et al., 2010). Proliferating progenitors (SOX9+, PAX6+) from the DNE are guided by and migrate together with TBR2+ (Eomes+) intermediate progenitors along the DMS to the final position of the dentate gyrus, where proliferation continues (Fig. 3A; Nelson et al., 2020). The DNE, the migration path and the final destination are termed the primary, secondary and tertiary matrices, respectively (Altman and Bayer, 1990b; Sugiyama et al., 2013).

Upon loss of β-catenin in the hem, both TBR2+ and PAX6+ progenitors were found to accumulate in the ectopic protrusion that contained the fimbrial glia and CR cells, instead of migrating along the DMS (Fig. 3A,B). LEF1, a factor necessary for dentate granule fate (Galceran et al., 2000), marks a population in the DNE that migrates to the tertiary matrix in controls. In Lmx1aCre::β-catenin LOF brains, LEF1+ cells accumulated close to the ectopic CR cell cluster, and very few migrated to their final destination at the hippocampal fissure (Fig. 3C). Finally, PROX1+ dentate granule cells failed to form the characteristic 'V' shape of the dentate gyrus in β-catenin LOF brains and appear to be arrested and juxtaposed to the ectopic and disorganized fimbrial glial protrusion (Fig. 3E,F). We quantified the percentage of TBR2+ and PROX1+ cells that reached the tertiary matrix/dentate gyrus or were mislocalized in the region of the hem/ventricular zone, and found that whereas the control brains had a negligible number of mislocalized cells, β-catenin LOF brains contained a significantly larger number in the ectopic site, and a significantly smaller number in the location of the future dentate gyrus (Fig. 3D,G; Fig. S6A-F). The TBR2+ intermediate progenitor population in the secondary and tertiary matrix of β-catenin LOF brains was similar to that in controls (Fig. S6D). However, the total number of PROX1 cells in the β-catenin LOF brain was significantly lower than that in controls (Fig. 3G; Fig. S6H), suggesting that reduced numbers of dentate gyrus progenitors were specified, or their proliferation/survival was affected. Dentate gyrus specification requires Wnt signaling from the hem (Lee et al., 2000). Although it appears that dentate gyrus cell fate was specified, at least in terms of PROX1, the underlying basis of the reduction in PROX1+ cells is an important angle for further studies focused on the mechanism of specification of dentate gyrus cells.

Both CR cells and the fimbrial scaffold glia are important in guiding the DMS (Stanfield and Cowan, 1979; Caramello et al., 2021). When chemokine signaling from CR cells is disrupted in either CXCR4 or CXCL12 (SDF-1) mutants (Bagri et al., 2002; Lu et al., 2002), the DMS is perturbed. The CR cells are themselves guided by the fimbrial glial scaffold. When this scaffold is ablated from E13.5 using diphtheria toxin fragment A (DTA) driven by hem-specific Fzd10Cre, CR cell migration is aberrant and these cells are scattered in ectopic locations (Gu et al., 2011). To test the requirement for β-catenin specifically in the CR cells, we used Foxj1Cre, which is selective for these cells and does not drive recombination in the fimbrial scaffold (Fig. 3H). Foxj1Cre::β-catenin LOF brains showed no defect in CR cell localization in the hippocampal fissure and there was no apparent defect in the formation of the dentate gyrus (Fig. 3H,I).

In summary, we have identified that β-catenin function is essential in the hem-derived fimbrial glial scaffold (but not in hem-derived CR cells) for normal morphogenesis of the dentate gyrus. In the absence of β-catenin, the fimbrial glial scaffold is disorganized and forms an ectopic ventricular protrusion as early as E12.5, before the migration of PROX1+ dentate granule cells, which begins at E14.5. Both dentate granule cells and CR cells depend on the glial scaffold for their proper migration and both these cell types migrate into the protrusion instead (Fig. 4; Fig. S7; Movie 1). This disrupted migration does not improve with time, and the dentate gyrus fails to form. Therefore, the protrusion, which is composed of disorganized glial scaffold cells in Lmx1aCre::β-catenin LOF brains, is the major and proximate cause of the profoundly defective morphogenesis of the dentate gyrus. Although deficits in the organization of glia in the dentate region have been reported in some canonical Wnt pathway mutants such LRP6 and LEF1 (Zhou et al., 2004), neither of these, nor any known mutant that lacks a component of adherens junctions (Zhang et al., 2013), displays such extreme disorganization as that seen in Lmx1aCre::β-catenin LOF brains. These results highlight the function of a single factor, β-catenin, as a key regulator of fimbrial scaffold organization, which ultimately controls the morphogenesis of a key hippocampal structure, the dentate gyrus.

MATERIALS AND METHODS

Mice

The Institutional Animal Ethics Committee of the Tata Institute of Fundamental Research Mumbai, India approved all animal protocols. All mice strains were maintained in an ambient temperature and humidity condition. The food and water were available *ad libitum* and a 12 h light/dark cycle was strictly followed. The Lmx1aCre mouse line described in this study was a kind gift from Kathy Millen (Center for Integrative Brain Research, Seattle Children's Research Institute, WA, USA; Chizhikov and Millen, 2004). Foxj1Cre was provided by M.J.H. The β-catenin exon 2-6 floxed mouse line (Brault et al., 2001) was obtained from Raj Awatramani (Department of Neurology and Center for Genetic Medicine, Northwestern University Feinberg Medical School Chicago, IL, USA). The Ai9 reporter mouse line was obtained from The Jackson Laboratory (Stock No. 007909). Noon of the day when the vaginal plug was observed was defined as E0.5. Only male animals were used for analysis because in the Lmx1aCre animals the transgene is located on the X-chromosome and, in females, it shows a mosaic expression of the Cre due to random X inactivation. For Foxj1Cre

Development (2022) 149, dev200953. doi:10.1242/dev.200953

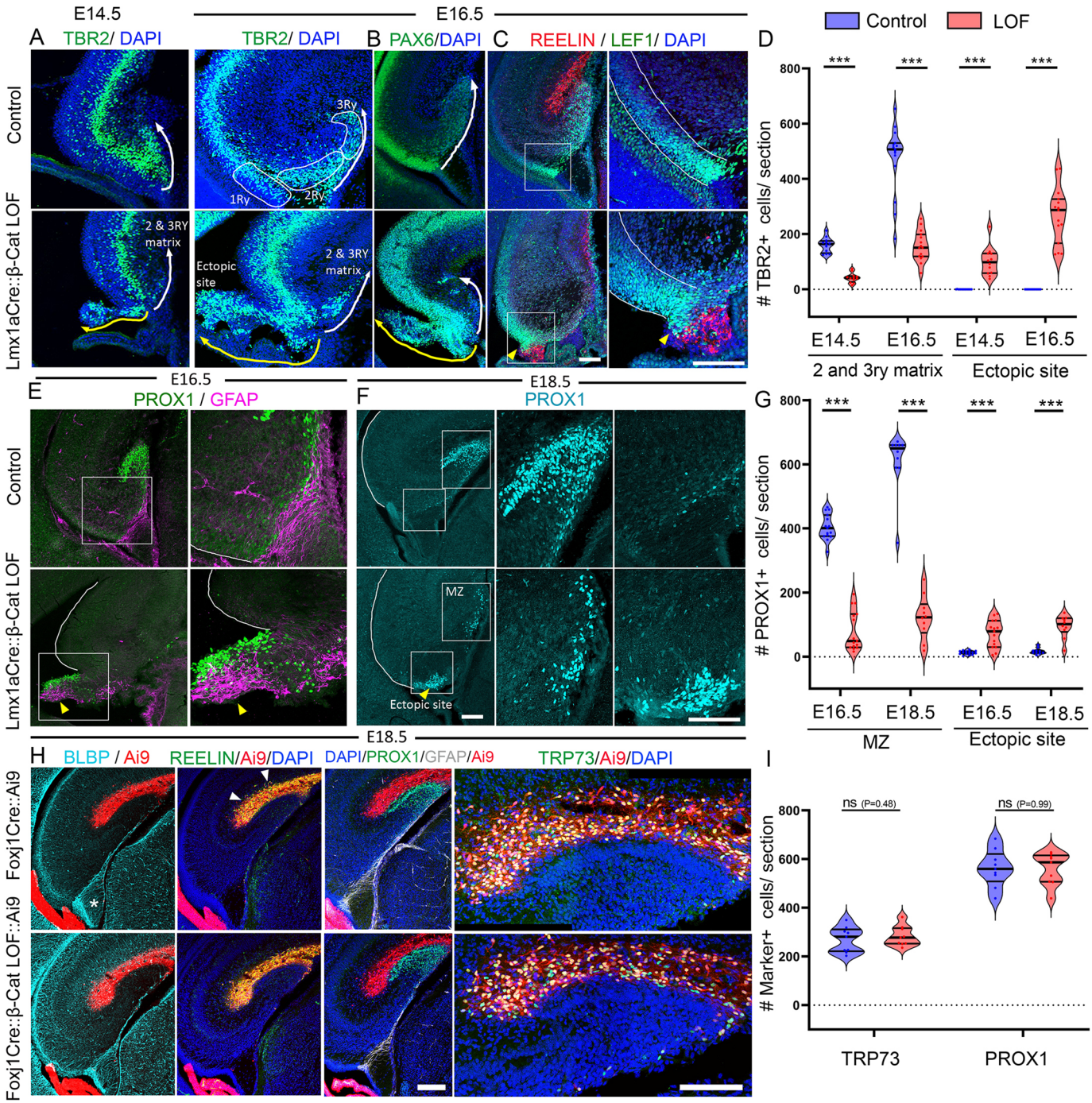

Fig. 3. Loss of β-catenin in cortical hem leads to mis-migration of the dentate migratory stream resulting in defective dentate gyrus morphogenesis. (A,B) TBR2+ and PAX6+ progenitors are seen in the secondary (2) and tertiary (3RY) matrices of the DMS at E14.5 and E16.5 in control brains (DMS, white arrow). In Lmx1aCre::β-catenin LOF brains, these cells are diverted to the ectopic glial protrusion (yellow arrow); representative images are shown of sections taken from *N*=4 (E14.5) and *N*=5 (E16.5) brains (biologically independent replicates) examined over three independent experiments. White outlines indicate primary (1RY), secondary (2RY) and tertiary (3RY) matrices. (C) In control brains, reelin+ CR cells reside in the hippocampal fissure above LEF1+ DMS cells, whereas in β-catenin LOF brains both these cell types are co-mingled in the ectopic protrusion (yellow arrowhead). (D) Quantification of the images in A. *N*=4 (E14.5); *N*=5 (E16.5) biologically independent replicates examined over three independent experiments. (E,F) PROX1+ dentate granule cells localize to the dentate gyrus in controls, but are diverted to the ectopic protrusion in β-catenin LOF brains (yellow arrowhead). The boxed region in C, E and F are shown in high magnification in the panels on the right. (G) Quantification of the images in E and F. *N*=5 (E16.5 and E18.5) biologically independent replicates examined over three independent experiments. (H) FoxJ1Cre does not drive Ai9 reporter expression in the BLBP+ fimbrial scaffold (asterisk) but efficiently labels the reelin+ CR cells (white arrowheads). At E18.5, PROX1+ dentate granule cells and TRP73+ CR cells appear to be normally positioned in both control and Foxj1Cre::β-catenin LOF brains. (I) Quantification of the images in H. *N*=3 (E18.5) biologically independent replicates examined over three independent experiments. In A and H, image stitching was performed (see Materials and Methods: Image acquisition and analysis for details). Statistical tests (D,G,I): two-tailed unpaired Mann–Whitney *U*-test; ***$P<0.001$; ns, $P>0.05$ [E: $P=0.9268$; G: $P=0.000011$ (E16.5 and E18.5 MZ), $P=0.000084$ (E16.5 ectopic site), $P=0.000076$ (E18.5 ectopic site)]. Scale bars: 100 µm.

Development (2022) 149, dev200953. doi:10.1242/dev.200953

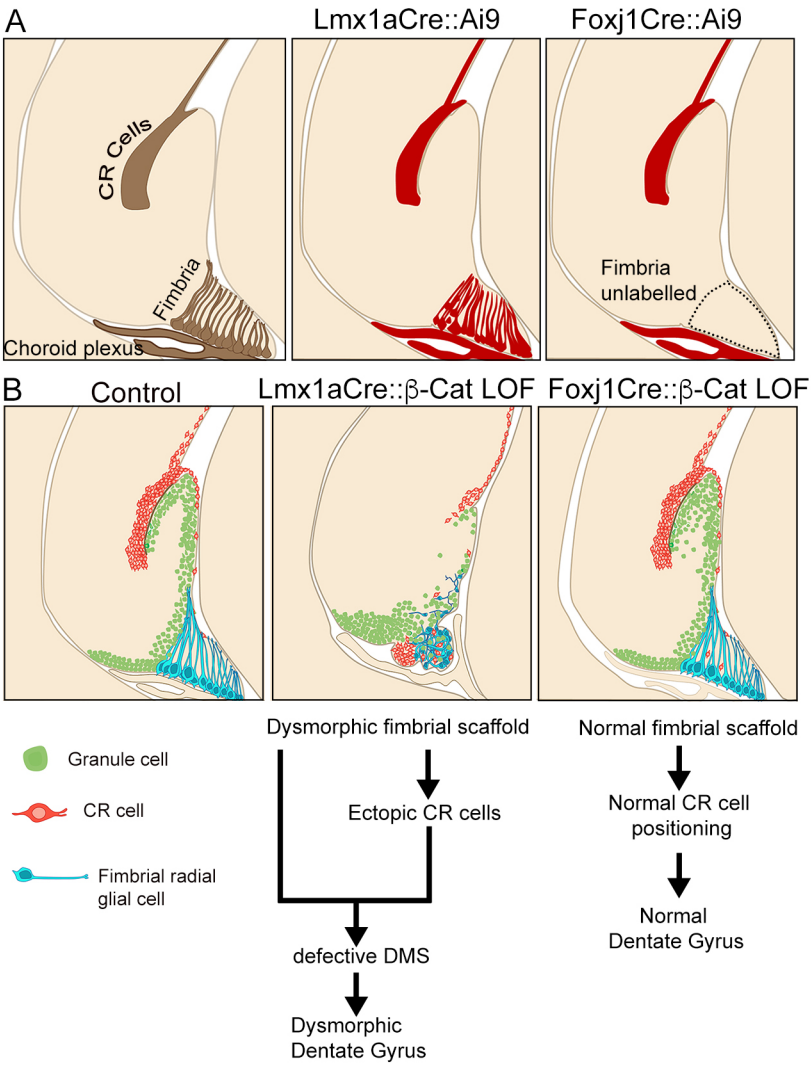

Fig. 4. Schema depicting β-catenin LOF phenotypes associated with Lmx1aCre or Foxj1Cre drivers. (A) The cartoons illustrate all three hem-derived lineages (brown), i.e. the choroid plexus, CR cells, and the fimbrial scaffold in the E18.5 hippocampus, which also displays the Ai9 reporter (red) when recombined with Lmx1Cre. Foxj1Cre drives recombination in the CR cells and the choroid plexus but not in the fimbrial scaffold. (B) Cartoon of the control, Lmx1aCre::β-catenin LOF and Foxj1Cre::β-catenin LOF hippocampus showing the dentate migratory stream (green), the fimbrial scaffold (blue) and CR cells (orange) in the hippocampal fissure. In the Lmx1aCre::β-catenin LOF brain, fimbrial scaffold is disorganized, resulting in CR cells and dentate migratory cells accumulating in an ectopic protrusion. No such disruption is seen in the Foxj1Cre:: β-catenin LOF hippocampus.

experiments, both male and female embryos were analyzed. All the controls described in the study were littermates unless otherwise stated. The following primer sets were used for genotyping: Cre FP: 5′ATTT-GCCTGCATTACCGGTC3′; Cre RP: 5′ATCAACGTTTTCTTTTCGG3′. A Cre+ band can be seen at 350 bp. For genotyping of the β-catenin LOF mouse (exon 2-6 floxed) the following combination of primers was used: RM41 5′AAGGTAGAGTGATGAAAGTTGTT3′; RM42 5′CACCATGT-CCTCTGTCTATTC3′; RM43 5′TACACTATTGAATCACAGGGACTT3′. This PCR exhibits a wild-type band at 221 bp and a floxed band at 324 bp (Brault et al., 2001).

Immunohistochemistry

Mouse brain coronal sections were mounted on plus slides (Electron Microscopy Sciences, 71869-11) and dried for 2-3 h on a slide drier. Slides were then transferred to a slide mailer (Electron Microscopy Sciences, 71549-08) and washed with a solution containing PBS+0.01% Triton X-100 for 10 min. Further, the slides were washed with PBS+0.03% Triton X-100 for 5 min (twice). Antigen retrieval was performed in a water bath. In this step, a 10 mM sodium citrate buffer (pH 6) was used and the slides were incubated at 90°C for 10 min inside the water bath. The slide mailer was left for 20 min at room temperature for cooling and further washed with PBS+0.01% Triton X-100 for 5 min (twice). A blocking solution containing 5% horse serum in PBS+0.3% Triton X-100 was added and slides were incubated for 1 h in a humidified box. This step was followed by overnight primary antibody incubation at 4°C (cold room). The next day secondary antibody incubation was carried out at room temperature for 2 h in a humidified box covered with aluminum foil. Two washes with 1× PBS were performed on a rocker followed by incubation with DAPI (Invitrogen, 62248). Slides were mounted using Fluoroshield mounting media (Sigma-Aldrich, F6182) and imaged using an Olympus FluoView 1200 confocal microscope. The primary antibodies used were: LEF1 [rabbit, 1:200, Cell Signaling Technology (CST), C12A5], β-catenin (mouse, 1:200, BD Biosciences, 610153), β-catenin (rabbit, 1:50, CST, 8814), RFP (rabbit, 1:200, Abcam, ab62341), RFP (mouse, 1:200, Invitrogen, MA5-15257), TBR2 (rabbit, 1:200, Abcam, ab23345), TBR2 (rat, 1:200, Invitrogen, 14-4875-82), PAX6 (rabbit, 1:500, Abcam, ab195045), PROX1 (rabbit, 1:500, Millipore, ab5475), BLBP (rabbit, 1:200, Sigma-Aldrich, ABN14), TRP73 (rabbit, 1:200, CST, 14620S), reelin (mouse, 1:200, Millipore, MAb5364), TTR (rabbit, 1:75, Dako, A0002), GFAP (rabbit, 1:200, Sigma-Aldrich, G9269), GFAP (mouse, 1:200, Sigma-Aldrich, G3893), N-cadherin (mouse, 1:200, BD Biosciences, 610920), NEUROD1 (rabbit, 1:1000, Abcam, AB213725), Phospho histone H3 (rabbit, 1:200, CST, H0412), Ki67 (rabbit, 1:200, Abcam, ab15580), SOX9 (rabbit, 1:200, Abcam, ab185230), SOX2 (mouse, 1:200, Invitrogen, MA1-014), NFIA (rabbit, 1:500 Abcam, ab228897), NFIB (rabbit, 1:500, Abcam, ab186738), ALDH1L1 (rabbit, 1:200, Abcam, ab87117), AQP4 (rabbit, 1:200, CST, 59678). Secondary antibodies used in this study were: goat anti-rabbit Alexa fluor 488 (1:200, Invitrogen, A11034), goat anti-mouse Alexa fluor 594 (1:200, Invitrogen, R37121), goat anti-rabbit Alexa fluor 568 (1:200, Invitrogen, A11011), donkey anti-rabbit Alexa fluor 647 (1:200, Invitrogen, A31573), goat anti-mouse Alexa fluor 647 (1:200, Invitrogen, A21236), goat anti-mouse Alexa fluor 488 (1:200, Invitrogen, A28175), goat anti-rat Alexa fluor 488 (1:200, Invitrogen, A11006).

Development (2022) 149, dev200953. doi:10.1242/dev.200953

In situ hybridization

Plasmids used to generate probes for *in situ* hybridization were kind gifts from Elizabeth Grove (University of Chicago, IL, USA; *Lmx1a*, *Wnt3a*, *Axin2*), and Cliff Ragsdale (University of Chicago, IL, USA; *Fzd1*). The detailed procedure of *in situ* hybridization has been previously described (Parichha et al., 2022).

Image acquisition and analysis

Bright-field images were acquired using a Zeiss Axioskop-2 plus microscope combined with a Nikon DS-fi2 camera and NIS Elements V4.0 software. Mouse sections were imaged using an Olympus FluoView 1200 confocal microscope with FluoView software. All the image analysis was carried out in Fiji-ImageJ and/or Adobe Photoshop CS6. Three-dimensional reconstruction (Fig. S4, Movie 1) was performed in Imaris (V7.2.3). In Fig. 3A and H, image stitching was performed using the 'pairwise stitching' plugin in Fiji. For all stitching operations 'subpixel accuracy' parameter was selected. Nonlinear operation such as gamma correction was not performed in any of the figures. Brightness and contrast adjustments were performed identically for control and mutant conditions. For Fig. 2E and F, cell counting was performed using the 'cell counter' plugin in Fiji. Three sections from different rostro-caudal levels were scored for each brain. A 317×137 µm region of interest (ROI) was placed along the hippocampal marginal zone of coronal sections to score the cells and was designated 'MZ' (Fig. 2F). Any cells outside that defined ROI were considered as 'outside MZ'. Three sections spread over different rostro-caudal levels per brain were quantified. To quantify the NCAD distribution in Fig. 2K and Fig. S5D,E, a line (3.5 µm in length) was placed across the cell boundary when the BLBP channel was selected. Ten such ROIs were placed per brain and the intensity profiles were plotted from the NCAD channel using the 'multiplot' option in the ROI manager. Every fourth slice of a *z*-stack was used for quantification. For Fig. 3D, TBR2+ cells in the secondary and tertiary matrices were counted using the 'cell counter' plugin. The 'C' shaped curve of the section where the ventricular zone ends is considered as the beginning of the secondary and tertiary matrices. The 'ectopic site' in the Lmx1aCre::β-catenin LOF brains refers to the prominent blob protruding in the ventricles. Three sections spread over different rostro-caudal levels per brain were quantified. In Fig. S1, quantification of number of PHH3+SOX2+Ai9+ cells (H) and Ki67+SOX2+Ai9+ (I) cells was carried out using the 'cell counter' plugin in Fiji. All the schematics were prepared using Microsoft PowerPoint 2016 and Adobe Photoshop 2017.

RNA-sequencing and analysis

All dissections were performed in ice-cold PBS. For dissecting hem, the telencephalic hemispheres were isolated using #5 forceps under a stereo zoom microscope (Nikon SMZ445). The choroid plexus was gently removed from the telencephalic ventricle using blunt forceps. Using fine tweezers the hem region was extracted (Fig. S3A). We examined the brains for Ai9 fluorescence before and after microdissection to ascertain that the Ai9+ hem was properly extracted (Fig. S3A). RNA extraction was performed using a standard Trizol reagent (Invitrogen, 15596026). Extracted RNA was analyzed for integrity using the Agilent 2100 bioanalyzer (RIN>7.5). Hem dissected from eight embryos was pooled for each of two biological replicates. Library preparation and sequencing were performed on the Illumina platform to achieve 100 bp or 150 bp reads to generate 30 million paired-end reads. The reads were quantified using Feature counts (Liao et al., 2014). Differential expression analysis was performed using DESeq2 on the R platform (v3.6.3).

Statistics and reproducibility

Biological replicates (*n*) denote samples obtained from individual embryos/pups. Blinded quantification was not possible for Lmx1aCre::β-catenin LOF brains because the mouse genotypes were easily distinguishable by distinct phenotypic features. For Foxj1Cre::β-catenin LOF brains, blinded analysis was performed. To avoid bias while analyzing the images, stringent measures are taken as described in the 'Image acquisition and analysis' section. All statistical analyses were performed in GraphPad Prism (V9.3.1). Information about the exact statistical test performed and *P*-value information is provided in corresponding figure legends. The distribution of the data points was analyzed using the Kolmogorov–Smirnov normality test. If the data were distributed normally then a parametric test was chosen, otherwise a non-parametric test was performed. For all statistical tests, the chosen confidence interval was always 95% (α=0.05). For all violin plots, the solid thick black line represents the median, solid thin black lines represent quartiles, and dots represent individual data points. For all the tests, outlier removal was not performed. For the *xy* plots in Fig. 2K and Fig. S5, error bars (shades) represent s.e.m. See supplementary Dataset 1 for all raw data points.

Acknowledgements

We thank Dr K. Millen (Seattle Children's Research Institute, WA, USA) for the kind gift of the Lmx1aCre line, Raj Awatramani (Department of Neurology and Center for Genetic Medicine, Northwestern University Feinberg Medical School Chicago, IL, USA) for the β-catenin CKO line. We thank Dr Shital Suryavanshi and the animal house staff of the Tata Institute of Fundamental Research for their excellent support. We acknowledge Ms Binita Vedak for her help in genotyping.

Competing interests

M.J.H. is the Founder and President of NuPeak Therapeutics and a member of the Data Safety Monitoring Board for AstraZeneca. All other authors declare no competing interests.

Author contributions

Conceptualization: A.P., S.T.; Methodology: A.P.; Software: V.S.; Validation: A.P., D.D.; Formal analysis: A.P., D.D., V.S.; Investigation: A.P., D.D., M.C.; Resources: M.J.H.; Data curation: A.P.; Writing - original draft: A.P.; Writing - review & editing: A.P., S.T.; Visualization: A.P., S.T.; Supervision: S.T.; Project administration: S.T.; Funding acquisition: S.T.

Funding

This work was supported by a Wellcome Trust-Department of Biotechnology India Alliance Early Career Fellowship (M.C., IA-E-12-1-500765); by the Canada-Israel Health Research Initiative, jointly funded by the Canadian Institutes of Health Research, the Israel Science Foundation, the International Development Research Centre, Canada and the Azrieli Foundation (S.T., 108875); intramural funds from Tata Institute of Fundamental Research–Department of Atomic Energy, Government of India (12-R&D-TFR-5.10-0100RTI2001); and a grant from Department of Science and Technology, Ministry of Science and Technology, Government of India (S.T.; DST/CSRI/2017/202). Deposited in PMC for release after 6 months.

Data availability

The mouse hem E12.5 RNA-seq data (Fig. S3) generated in this study have been deposited in the SRA database under the BioProject accession number PRJNA837732. See Table S1 for the list of differentially expressed genes.

Peer review history

The peer review history is available online at https://journals.biologists.com/dev/lookup/doi/10.1242/dev.200953.reviewer-comments.pdf.

References

Altman, J. and Bayer, S. A. (1990a). Migration and distribution of two populations of hippocampal granule cell precursors during the perinatal and postnatal periods. *J. Comp. Neurol.* **301**, 365-381. doi:10.1002/cne.903010304

Altman, J. and Bayer, S. A. (1990b). Mosaic organization of the hippocampal neuroepithelium and the multiple germinal sources of dentate granule cells. *J. Comp. Neurol.* **301**, 325-342. doi:10.1002/cne.903010302

Bagri, A., Marín, O., Plump, A. S., Mak, J., Pleasure, S. J., Rubenstein, J. L. R. and Tessier-Lavigne, M. (2002). Slit proteins prevent midline crossing and determine the dorsoventral position of major axonal pathways in the mammalian forebrain. *Neuron* **33**, 233-248. doi:10.1016/S0896-6273(02)00561-5

Barry, G., Piper, M., Lindwall, C., Moldrich, R., Mason, S., Little, E., Sarkar, A., Tole, S., Gronostajski, R. M. and Richardse, L. J. (2008). Specific glial populations regulate hippocampal morphogenesis. *J. Neurosci.* **28**, 12328-12340. doi:10.1523/JNEUROSCI.4000-08.2008

Brault, V., Moore, R., Kutsch, S., Ishibashi, M., Rowitch, D. H., Mcmahon, A. P., Sommer, L., Boussadia, O. and Kemler, R. (2001). Inactivation of the (β)-catenin gene by Wnt1-Cre-mediated deletion results in dramatic brain malformation and failure of craniofacial development. *Development* **128**, 1253-1264. doi:10.1242/dev.128.8.1253

Bunt, J., Osinski, J. M., Lim, J. W., Vidovic, D., Ye, Y., Zalucki, O., O'connor, T. R., Harris, L., Gronostajski, R. M., Richards, L. J. et al. (2017).

Combined allelic dosage of *Nfia* and *Nfib* regulates cortical development. *Brain Neurosci. Adv.* **1**, 2398212817739433. doi:10.1177/2398212817739433

Caramello, A., Galichet, C., Rizzoti, K. and Lovell-Badge, R. (2021). Dentate gyrus development requires a cortical hem-derived astrocytic scaffold. *eLife* **10**, 1-33. doi:10.7554/eLife.63904

Chizhikov, V. V. and Millen, K. J. (2004). Control of roof plate formation by Lmx1a in the developing spinal cord. *Development* **131**, 2693-2705. doi:10.1242/dev.01139

Chizhikov, V. V., Lindgren, A. G., Mishima, Y., Roberts, R. W., Aldinger, K. A., Miesegaes, G. R., Spencer Currle, D., Monuki, E. S. and Millen, K. J. (2010). Lmx1a regulates fates and location of cells originating from the cerebellar rhombic lip and telencephalic cortical hem. *Proc. Natl. Acad. Sci. U.S.A.* **107**, 10725-10730. doi:10.1073/pnas.0910786107

Galceran, J., Miyashita-Lin, E. M., Devaney, E., Rubenstein, J. L. and Grosschedl, R. (2000). Hippocampus development and generation of dentate gyrus granule cells is regulated by LEF1. *Development* **127**, 469-482. doi:10.1242/dev.127.3.469

Gu, X., Liu, B., Wu, X., Yan, Y., Zhang, Y., Wei, Y., Pleasure, S. J. and Zhao, C. (2011). Inducible genetic lineage tracing of cortical hem derived CR cells reveals novel properties. *PLoS ONE* **6**, e28653. doi:10.1371/journal.pone.0028653

Gumbiner, B. M. (2005). Regulation of cadherin-mediated adhesion in morphogenesis. *Nat. Rev. Mol. Cell Biol.* **6**, 622-634. doi:10.1038/nrm1699

Hirano, S. and Takeichi, M. (2012). Cadherins in brain morphogenesis and wiring. *Physiol. Rev.* **92**, 597-634. doi:10.1152/physrev.00014.2011

Kadowaki, M., Nakamura, S., Machon, O., Krauss, S., Radice, G. L. and Takeichi, M. (2007). N-cadherin mediates cortical organization in the mouse brain. *Dev. Biol.* **304**, 22-33. doi:10.1016/j.ydbio.2006.12.014

Lavado, A., Lagutin, O. V., Chow, L. M. L., Baker, S. J. and Oliver, G. (2010). Prox1 Is required for granule cell maturation and intermediate progenitor maintenance during brain neurogenesis. *PLoS Biol.* **8**, 43-44. doi:10.1371/journal.pbio.1000460

Lee, S. M., Tole, S., Grove, E. and Mcmahon, A. P. (2000). A local Wnt-3a signal is required for development of the mammalian hippocampus. *Development* **127**, 457-467. doi:10.1242/dev.127.3.457

Lehtinen, M. K., Zappaterra, M. W., Chen, X., Yang, Y. J., Hill, A. D., Lun, M., Maynard, T., Gonzalez, D., Kim, S., Ye, P. et al. (2011). The cerebrospinal fluid provides a proliferative niche for neural progenitor cells. *Neuron* **69**, 893-905. doi:10.1016/j.neuron.2011.01.023

Liao, Y., Smyth, G. K. and Shi, W. (2014). featureCounts: an efficient general purpose program for assigning sequence reads to genomic features. *Bioinformatics* **30**, 923-930. doi:10.1093/bioinformatics/btt656

Loo, L., Simon, J. M., Xing, L., Mccoy, E. S., Niehaus, J. K., Guo, J., Anton, E. S. and Zylka, M. J. (2019). Single-cell transcriptomic analysis of mouse neocortical development. *Nat. Commun.* **10**, 134. doi:10.1038/s41467-018-08079-9

Louvi, A., Yoshida, M. and Grove, E. A. (2007). The derivatives of the Wnt3a lineage in the central nervous system. *J. Comp. Neurol.* **504**, 550-569. doi:10.1002/cne.21461

Lu, M., Grove, E. A. and Miller, R. J. (2002). Abnormal development of the hippocampal dentate gyrus in mice lacking the CXCR4 chemokine receptor. *Proc. Natl. Acad. Sci. USA* **99**, 7090-7095. doi:10.1073/pnas.092013799

Nakajima, K., Mikoshiba, K., Miyata, T., Kudo, C. and Ogawa, M. (1997). Disruption of hippocampal development in vivo by CR-50 mAb against Reelin. *Proc. Natl. Acad. Sci. USA* **94**, 8196-8201. doi:10.1073/pnas.94.15.8196

Nelson, B. R., Hodge, R. D., Daza, R. A. M., Tripathi, P. P., Arnold, S. J., Millen, K. J. and Hevner, R. F. (2020). Intermediate progenitors support migration of neural stem cells into dentate gyrus outer neurogenic niches. *eLife* **9**, e53777. doi:10.7554/eLife.53777

Parichha, A., Suresh, V., Chatterjee, M., Kshirsagar, A., Ben-Reuven, L., Olender, T., Taketo, M. M., Radosevic, V., Bobic-Rasonja, M., Trnski, S. et al. (2022). Constitutive activation of canonical Wnt signaling disrupts choroid plexus epithelial fate. *Nat. Commun.* **13**, 633. doi:10.1038/s41467-021-27602-z

Stanfield, B. B. and Cowan, W. M. (1979). The morphology of the hippocampus and dentate gyrus in normal and reeler mice. *J. Comp. Neurol.* **185**, 393-422. doi:10.1002/cne.901850302

Sugiyama, T., Osumi, N. and Katsuyama, Y. (2013). The germinal matrices in the developing dentate gyrus are composed of neuronal progenitors at distinct differentiation stages. *Dev. Dyn.* **242**, 1442-1453. doi:10.1002/dvdy.24035

Valenta, T., Gay, M., Steiner, S., Draganova, K., Zemke, M., Hoffmans, R., Cinelli, P., Aguet, M., Sommer, L. and Basler, K. (2011). Probing transcription-specific outputs of β-catenin in vivo. *Genes Dev.* **25**, 2631-2643. doi:10.1101/gad.181289.111

Valenta, T., Hausmann, G. and Basler, K. (2012). The many faces and functions of β-catenin. *EMBO J.* **31**, 2714-2736. doi:10.1038/emboj.2012.150

Zhang, J., Shemezis, J. R., Mcquinn, E. R., Wang, J., Sverdlov, M. and Chenn, A. (2013). AKT activation by N-cadherin regulates beta-catenin signaling and neuronal differentiation during cortical development. *Neural Dev.* **8**, 7. doi:10.1186/1749-8104-8-7

Zhou, C.-J., Zhao, C. and Pleasure, S. J. (2004). Wnt signaling mutants have decreased dentate granule cell production and radial glial scaffolding abnormalities. *J. Neurosci.* **24**, 121-126. doi:10.1523/JNEUROSCI.4071-03.2004

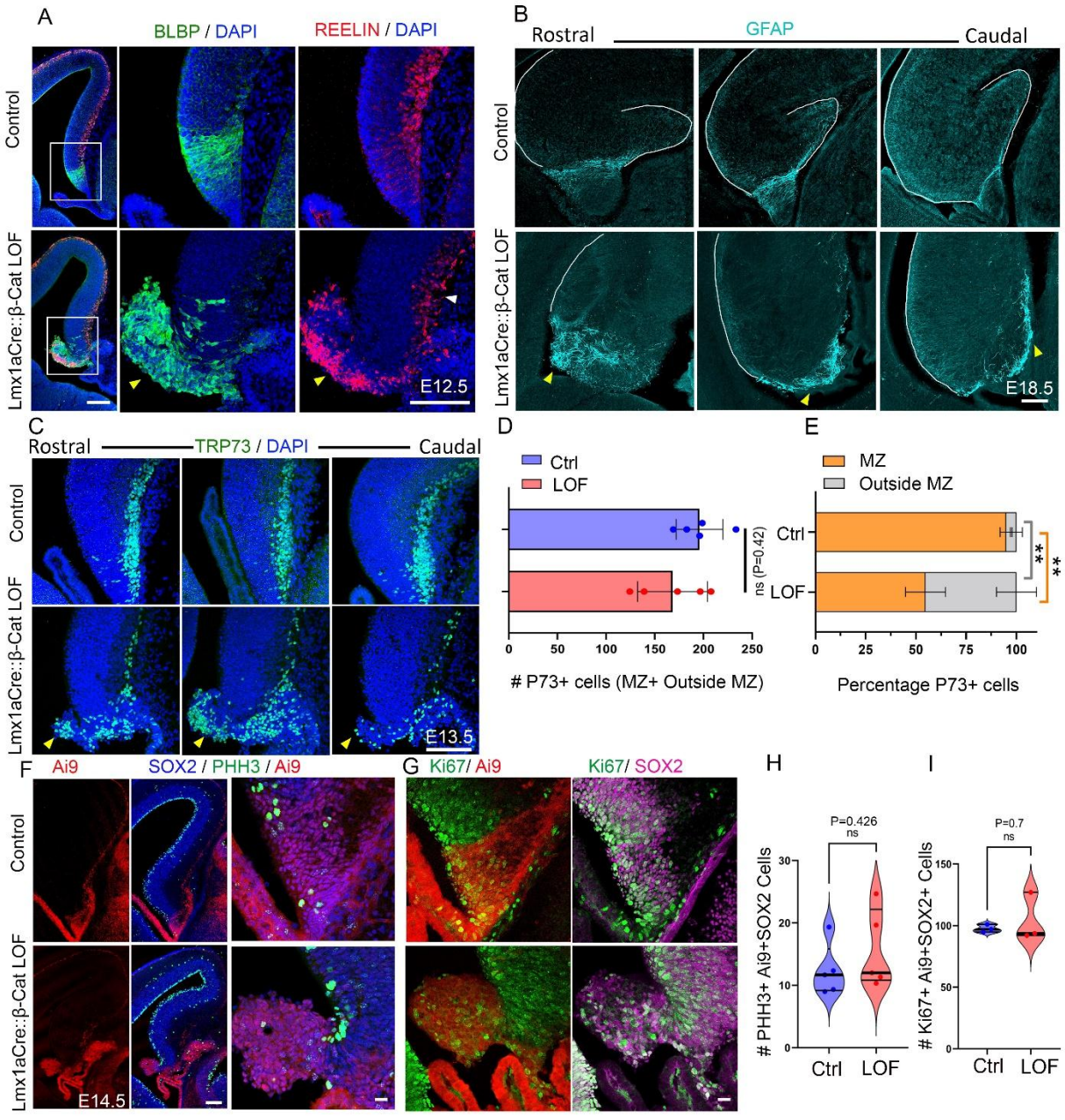

Fig. S1. Loss of β-CATENIN in the cortical hem causes dysmorphia of the fimbrial scaffold and mispositioning of the CR cells. (A) Co-immunolabeling for REELIN and BLBP at E12.5 reveals a disorganized fimbrial scaffold and mislocalized CR cells in Lmx1aCre::β-Catenin LOF brains compared with controls. These images show the individual BLBP (green) and REELIN (red) channels of the image in Fig. 2C). (B) GFAP labeling at E18.5 reveals a well-ordered fimbrial scaffold in controls, but a disorganized

scaffold in the Lmx1aCre::β-Catenin LOF brains (yellow arrowheads) at multiple rostro caudal levels; N=3 brains (biologically independent replicates) examined over 2 independent experiments. (C) A rostro caudal series reveals that TRP73+ hem-derived CR cells are mislocalized to the ectopically protruding glial mass (yellow arrowheads) throughout the rostro caudal extent of the E13.5 brain. (D) A bar graph representing the total number of TRP73+ cells (Mz+ Outside Mz) shows no significant difference between Lmx1aCre::β-Catenin LOF and control brains. (E) A stacked percentage bar graph displays the altered distribution of TRP73+ cells in Lmx1aCre::β-Catenin LOF compared to controls; N=5 (D and E) brains (biologically independent replicates) examined over 4 independent experiments, bars represent mean±SEM. (F, G) Co-immunostaining for proliferation markers PHH3 and Ki67, and progenitor marker SOX2 (H, I) Violin plots showing quantification of number of PHH3+SOX2+Ai9+ cells (H) and Ki67+SOX2+Ai9+ cells (I) reveal no change in proliferation in Lmx1aCre::β-Catenin LOF brains. Statistical tests (D, E, H and I): Two-tailed unpaired Mann Whitney U test, * $p < 0.05$, ** $p < 0.01$, *** $p < 0.001$, ns if p-value> 0.05; P=0.42 (D), P=0.0079 (E), P=0.426 (H), and P=0.7 (I). All scale bars: 100 μm.

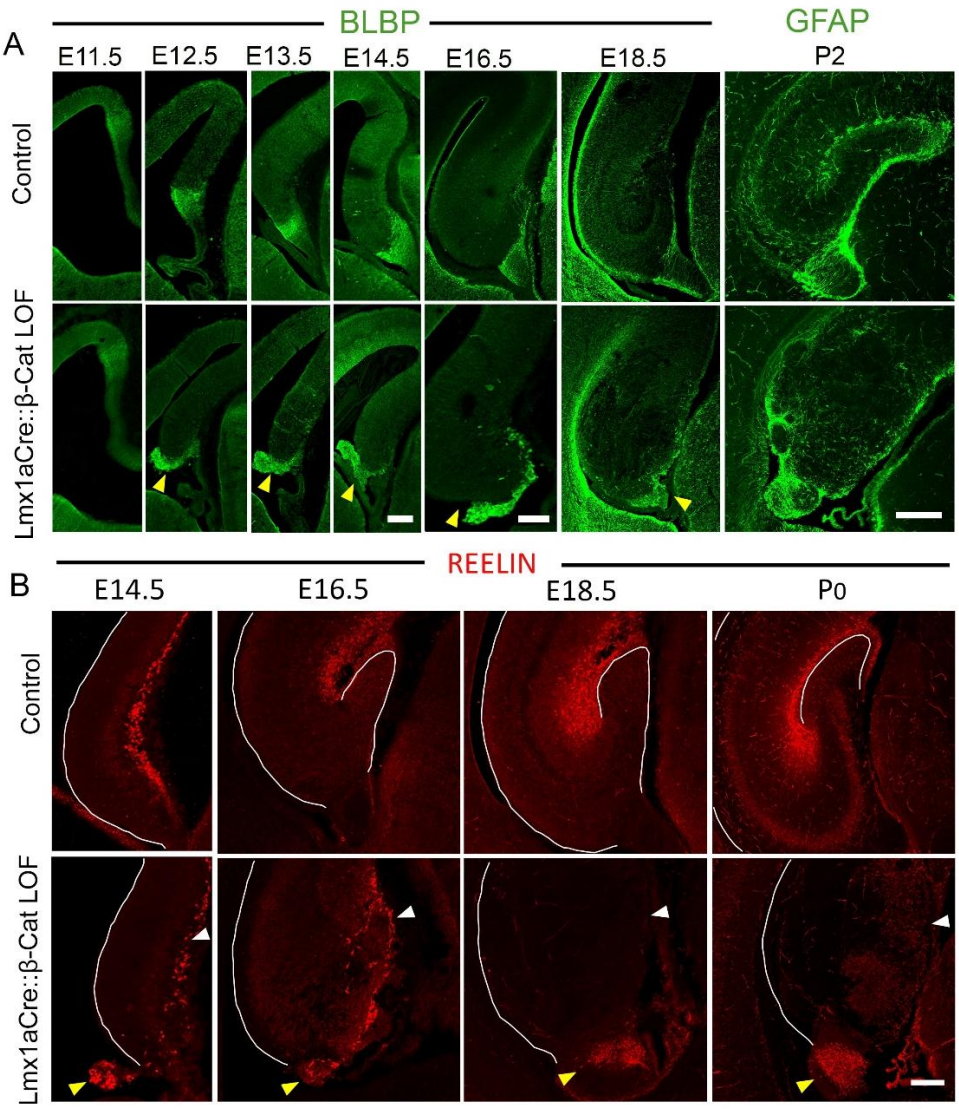

Fig. S2. No improvement of the β-Catenin LOF fimbrial scaffold disruption or CR cell mispositioning during late embryonic development. (A) BLBP (E11.5-E18.5) and GFAP (P2) immunolabeling show a well-organized fimbrial scaffold in controls, but a misoriented and disorganized scaffold in the Lmx1aCre::β-Catenin LOF brains; N=3 (E11.5) N=4 (E12.5); N=5 (E13.5 and E14.5), N=4 (E16.5 and E18.5), N=3 (P2) brains (biologically independent replicates) examined over 2 independent experiments. (B) Immunostaining for REELIN at E14.5, E16.5, E18.5 & P0 reveals no improvement in the mislocalized CR cells in the Lmx1aCre::β-Catenin LOF brains

during development (Marginal zone: white arrowheads, ectopic localization: yellow arrowheads); N=3 (E14.5); N=5 (E16.5), N=3 (E18.5), N=3 (P0) brains (biologically independent replicates) examined over 3 independent experiments. All scale bars: 100 μm.

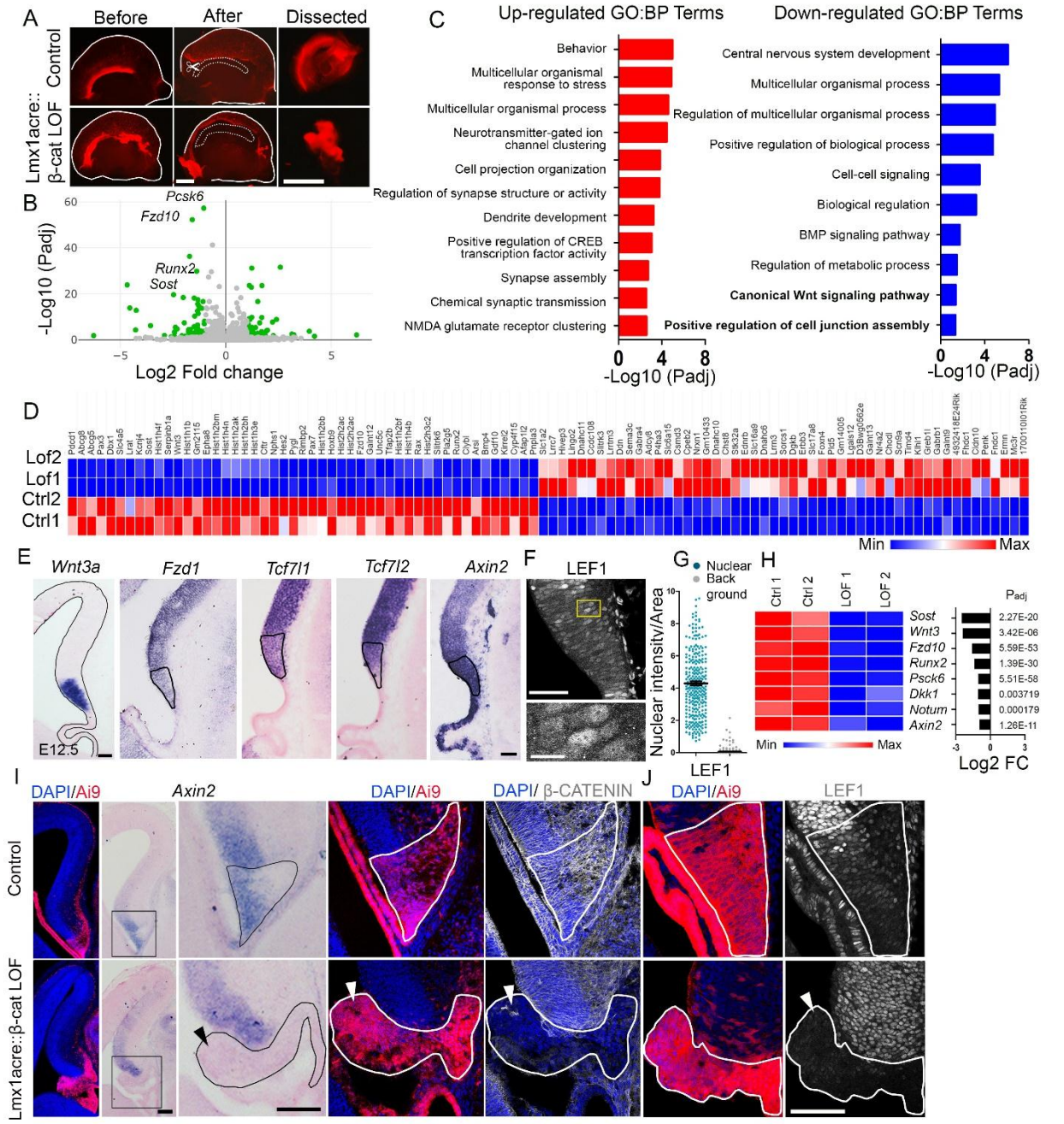

Fig. S3. Transcriptional changes associated with loss of β-CATENIN in the cortical hem. (A) Microdissection of E12.5 Ai9-labeled telencephalic hemispheres (before and after dissection) to obtain hem tissue for RNA sequencing. (B) A volcano plot showing differentially regulated genes (green dots represent genes with significantly changed expression). (C) Top 10 upregulated and downregulated GO: BP terms show down-regulation of “Canonical Wnt signaling pathway” and “Positive regulation of cell

junction assembly" in Lmx1aCre::β-Catenin LOF compared to controls. (D) Heat map representing Top 50 upregulated (red) and downregulated (blue) genes in control and Lmx1aCre::β-Catenin LOF brains; N=2 biological replicates. (E) The cortical hem, identified by *Wnt3a* expression, expresses several canonical Wnt pathway components such as *Fzd1, Tcf7l1, Tcf7l2*, and *Axin2* at E12.5, N=3 brains (biologically independent replicates) examined over 3 independent experiments. (F, G) immunostaining for Wnt target LEF1 and quantification. (H) Heatmap (displaying normalized reads) and Bar plots (showing log2 fold changes) of candidate Wnt pathway genes downregulated upon loss of β-CATENIN in the hem (complete data in supplementary table 1). (I) *In situ* hybridization for *Axin2* and immunolabeling for β-CATENIN in serial sections shows *Axin2* is undetectable (black arrowhead) at the same region where β-CATENIN staining is lost (Ai9 + area) in Lmx1aCre::β-Catenin LOF brains compared to controls. (J) LEF1 immunolabeling is almost undetectable (white outline) in Lmx1aCre::β-Catenin LOF hem (Ai9+ area). All scale bars: 100 μm.

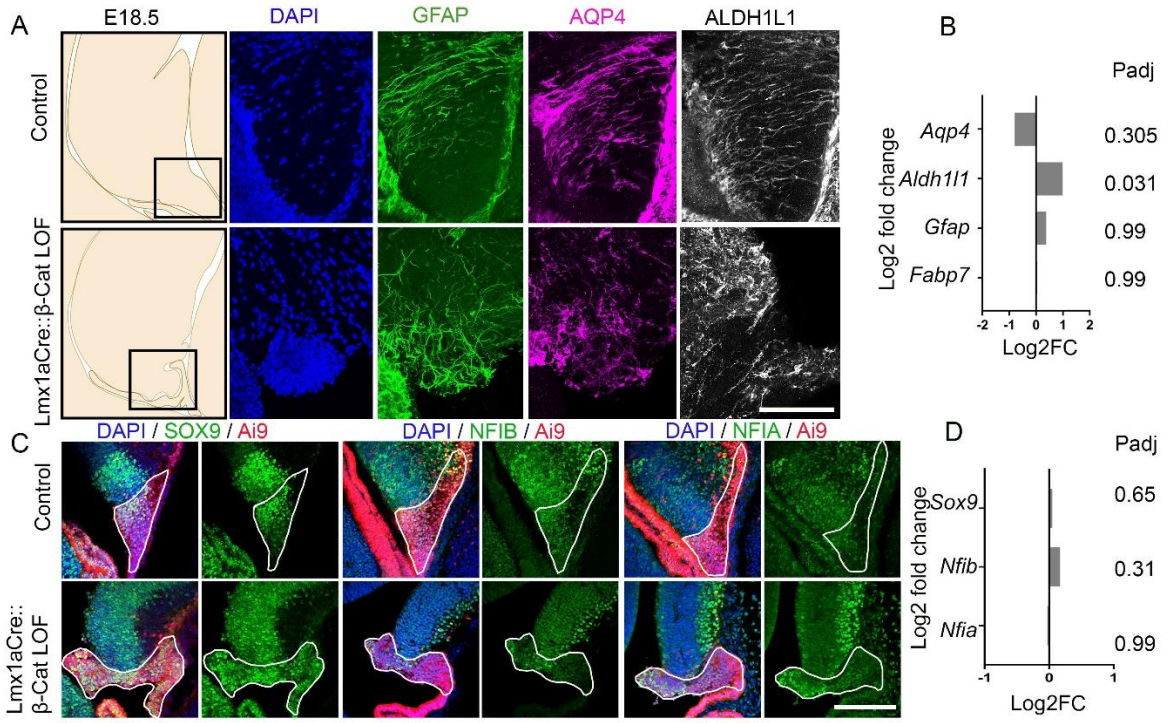

Fig. S4. Fimbrial scaffold markers and regulators maintain their expression upon loss of β-CATENIN. (A, B) The β-Catenin LOF fimbrial scaffold continues to display GFAP, AQP4, and ALDHL1 immunoreactivity (A), and expression of *Aqp4, Aldh1l1, Gfap, and Fabp7* is not significantly different (B) from that in control brains. (C) Immunostaining for SOX9, NFIA, and NFIB displays the presence of these regulators of fimbrial scaffold development and (D) Expression of *Sox9, Nfib, and Nfia* is not significantly altered in both control and β-Catenin LOF brains.

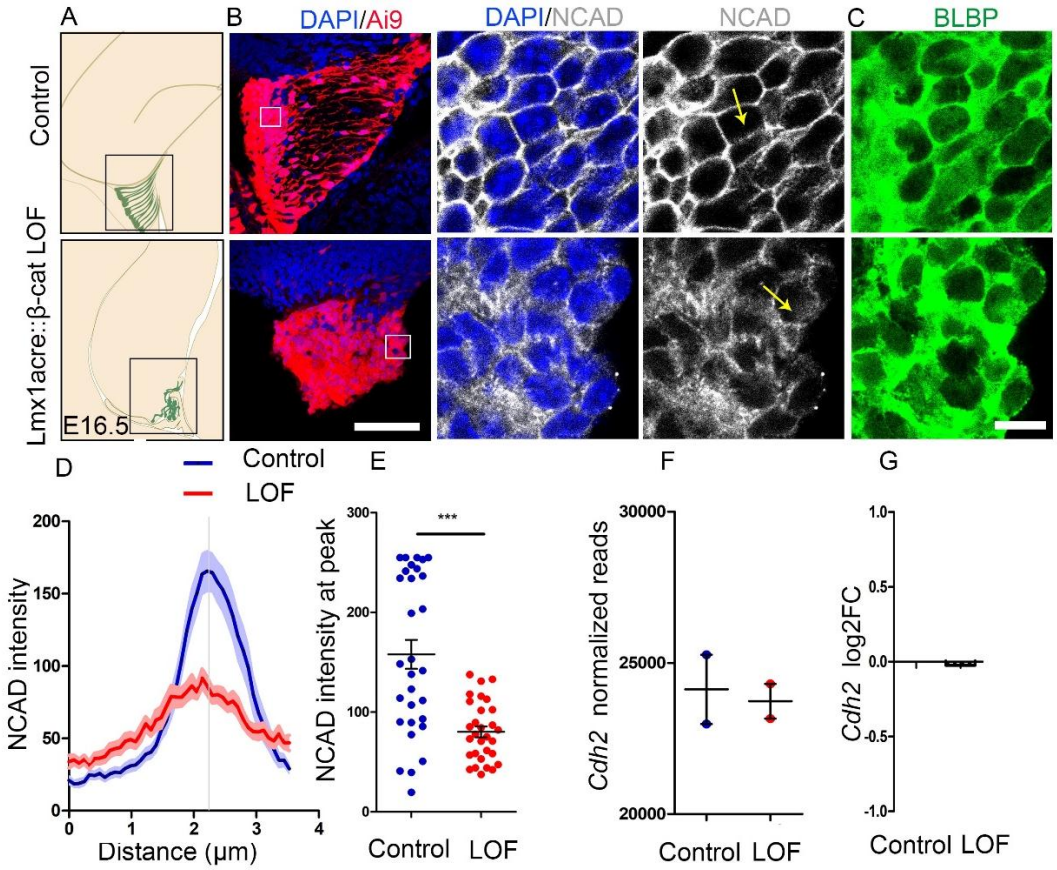

Fig. S5. Loss of β-CATENIN in cortical hem leads to altered cell-cell adhesion.

(A-C) Distribution of adherens junction marker N-CADHERIN and fimbrial scaffold marker BLBP in Ai9+ hem-derived cells. (B) High magnification images correspond to the boxed regions in the Ai9 image. (D, E) The intensity distribution of N-CADHERIN was quantitated across cell junctions (along the yellow arrow in the NCAD image). N= 3 brains (biologically independent replicates) examined over 3 independent experiments. (G) Normalized read counts (F) and log2 fold change for *Cdh2* gene, which encodes for NCAD, shows no significant change (p=0.99) between Lmx1aCre::β-Catenin LOF brains compared to controls. Statistical test: Two-tailed unpaired t-test with Welch correction (E) and Two-tailed unpaired Mann Whitney U test (D), * $p < 0.05$, ** $p < 0.01$, *** $p < 0.001$, ns if p-value> 0.05; P<0.0001 (E). Scale bars: 10 μm (C); 100 μm (B).

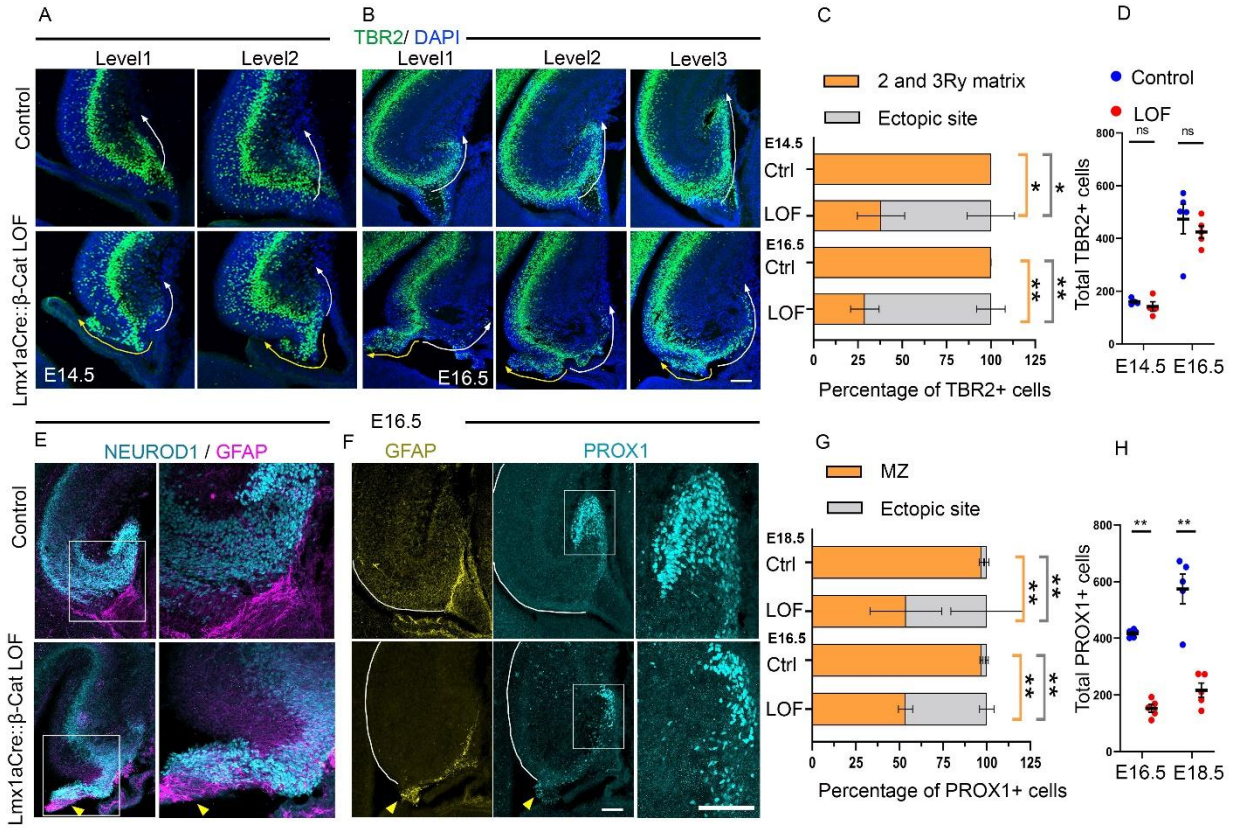

Fig. S6. The dentate migratory stream is diverted in the Lmx1aCre::β-Catenin LOF brains. (A, B) Sections at different rostro-caudal levels from E14.5 (A) and E16.5 (B) brains display TBR2+ cells in the 2ry & 3ry matrix of the dentate migratory stream in controls (white arrows). This migration is diverted to the ectopic glial protrusion in Lmx1aCre::β-Catenin LOF brains (yellow arrows). (C) Stacked percentage bar graphs displaying the altered distribution of TBR2+ dentate migratory cells in the 2ry & 3ry matrix vs the ectopic protrusion in Lmx1aCre::β-Catenin LOF brains compared to controls, N=4 (E14.5), N=5 (E16.5) brains (biologically independent replicates) examined over 3 independent experiments. (D) The total number of TBR2+ cells is not significantly different between Lmx1aCre::β-Catenin LOF and control brains. (E, F) At E16.5, Lmx1aCre::β-Catenin LOF brains display a disorganized GFAP+ fimbrial scaffold (yellow arrowheads) and mislocalized NEUROD1+ (E) and PROX1+ (F) dentate migratory cells. The boxed regions in E and F are shown at high magnification in the adjacent images. (G) Stacked percentage bar graphs displaying proportion of PROX1+

granule cells in the MZ (white box in F) vs the ectopic site (outside the white box) in the Lmx1aCre::β-Catenin LOF brains compared to controls, N=5 (E14.5 and E16.5) brains (biologically independent replicates) examined over 3 independent experiments. (H) The total number of PROX1+ granule cells is significantly lower in Lmx1aCre::β-Catenin LOF brains compared to controls. Stacked bar graphs (C and G) use the same data sets shown in the violin plots in Fig 3D and G. Error bars in C, D, G, and H represent SEM. Statistical test: Two-tailed unpaired Mann Whitney U test, * $p < 0.05$, ** $p < 0.01$, *** $p < 0.001$, ns if p-value> 0.05; P=0.028 (C, E14.5), P=0.0079 (C, E16.5), P=(0.3,E14.5; 0.15, E16.5), P= 0.007 (G, E16.5 and e18.5), and P=0.008 (H). All scale bars: 100 μm.

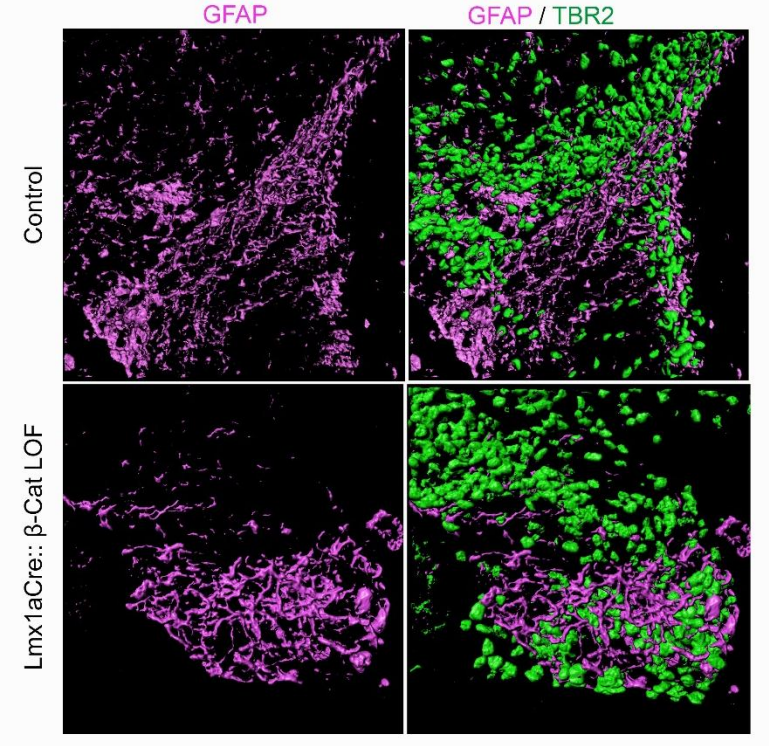

Fig. S7. A 3D reconstruction of the GFAP+ fimbrial scaffold and TBR2+ dentate migratory stream at E16.5. Upon loss of β-CATENIN the fimbrial scaffold is disorganized and the TBR2+ dentate migratory stream is diverted and intermingled with the disoriented fimbrial scaffold (see supplementary movie 1). Scale bar: 30μm.

Table S1. Normalized read counts and log2 fold changes with adjusted P values for the RNA seq data presented in Fig.S3, 4 & 5.

Click here to download Table S1

Supplementary dataset 1. Contains all the raw data points, statistical test summaries, and P value information corresponding to all the graphs shown in the main and the supplementary figures.

Click here to download Dataset 1

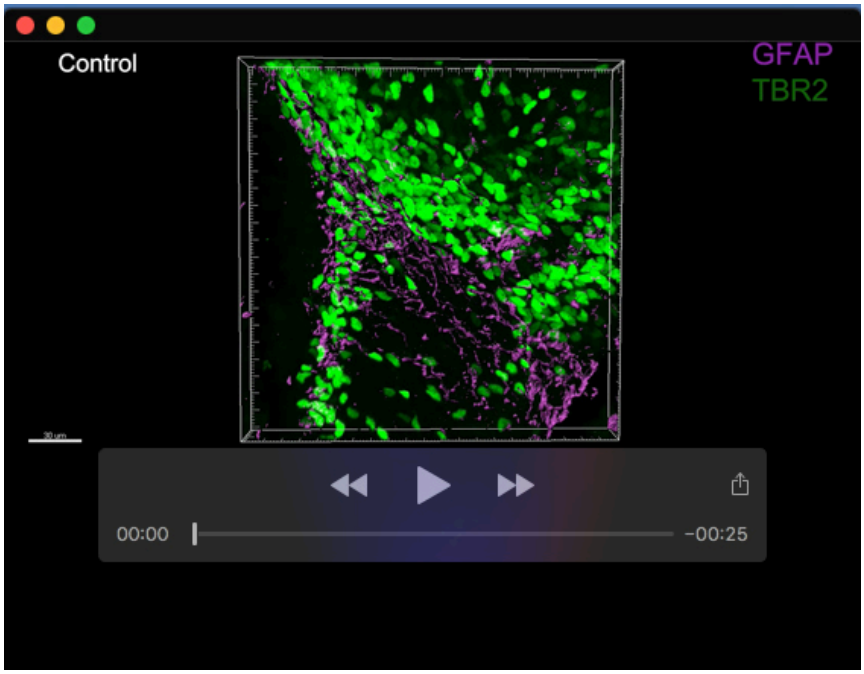

Movie 1. A movie corresponding to Fig. S7, generated using Imaris software, showing a 3D view of the GFAP+ fimbrial scaffold and the TBR2+ dentate migratory stream at E16.5. Loss of β-CATENIN leads to a disorganized fimbrial scaffold and diversion of the TBR2+ dentate migratory stream.